Comparative Analysis of Diagnostic Performance Between Elastography and AI-based S-detect for Thyroid Nodule Detection

Jee-Yeun Park and Sung-Hee Yang *

Posted Date: 3 July 2025

doi: 10.20944/preprints202411.0686.v2

Keywords: thyroid nodule; benign; malignant; elastography; thyroid ultrasonography

Peer-reviewed version available at Diagnostics 2025, 15, 2191; doi:https://doi.org/10.3390/diagnostics15172191

Article

Comparative Analysis of Diagnostic Performance Between Elastography and AI-Based S-Detect for Thyroid Nodule Detection

Jee-Yeun Park [1,2] and Sung-Hee Yang [2,*]

[1] Department of Radiological Science, Jangpalpal Internal Medicine Clinic, 369, Haeundae-ro, Haeundae-Gu, Busan 48062, Republic of Korea

[2] Department of Radiological Science, College of Health Sciences, Catholic University of Pusan, 46252 Busan, Republic of Korea

* Correspondence: sonoyang@cup.ac.kr; Tel.: +82-51-510-0582

Abstract

Objectives: This study aimed to evaluate the diagnostic performance and clinical utility of elastography and S-detect in distinguishing benign from malignant thyroid nodules. Elastography is a non-invasive imaging technique assesses tissue stiffness and elasticity. S-detect is a deep learning-based computer-aided diagnosis (DL-CAD) software that analyzes grayscale ultrasound 2D images to evaluate the morphological characteristics of thyroid nodules, providing a visual guide to the likelihood of malignancy. **Method:** This retrospective study included 159 patients who underwent thyroid ultrasonography between January 2023 and June 2024. All patients underwent elastography, S-detect analysis, and fine needle aspiration cytology (FNAC). Malignancy status was determined based on the FNAC findings and the diagnostic performance of elasticity contrast index (ECI), S-detect, and evaluations by a radiologist were assessed. Based on FNAC results, 101 patients (63.5%) had benign nodules and 58 patients (36.5%) had malignant nodules. **Results:** Radiologist interpretation demonstrated the highest diagnostic accuracy (area under the curve 89%), with a sensitivity of 98.28%, specificity of 79.21%, positive predictive value (PPV) of 73.1%, and negative predictive value (NPV) of 98.8%. The elasticity contrast index showed an accuracy of 85%, sensitivity of 87.93%, specificity of 81.19%, PPV of 72.9%, and NPV of 92.1%. S-detect yield the lowest accuracy at 78%, with a sensitivity of 87.93%, specificity of 68.32%, PPV of 61.4%, and NPV of 90.8%. **Conclusions:** Although limited by its single-center design and sample size, potentially limiting the generalization of the results, the controlled environment ensured consistency and minimized confounding variables. These findings offer valuable insights into the comparative diagnostic utility of Elastography and AI-based S-detect for thyroid nodules in clinical practice.

Keywords: thyroid nodule; benign; malignant; elastography; thyroid ultrasonography

1. Introduction

Thyroid cancer is one of the most common endocrine malignancies worldwide. According to the International Agency for Research on Cancer (IARC) under the World Health Organization (WHO), thyroid cancer accounts for approximately 87,000 new cases annually worldside, with an incidence rate ranging from 0.5 to 10 cases per 100,000 people. With the increasing prevalence of high-resolution ultrasound and routine medical examinations, the detection rate of thyroid nodules has significantly risen. Thyroid nodules are common clinical findings characterized by the overgrowth of thyroid cells and are detected in approximately 19–67% of the population through thyroid ultrasound. Approximately 5–15% of these cases are diagnosed as thyroid cancer [1–3]. As the detection of thyroid nodules increases, the frequency of thyroid cancer is also steadily increasing. Although the

Peer-reviewed version available at Diagnostics 2025, 15, 2191; doi:https://doi.org/10.3390/diagnostics15172191

occurrence of thyroid nodules cannot be completely prevented, regular health check-ups enable early detection and management.

The standard diagnostic approach for thyroid nodules includes physical examination, laboratiory assessments, thyroid nuclear scans, imaging modalities such as ultrasonography, and confirmatory procedures such as fine needle aspiration cytology (FNAC). Additional imaging techniques, such as computed tomography and magnetic resonance imaging, may be used if necessary [3–6]. Ultrasonography, in particular, is a highly useful, non-invasive, and convenient method for diagnosing thyroid lesions, as it not only detects nodules but also evaluates the involvement of surrounding lymph nodes and adjacent tissues [7]. The main disadvantage of the method is that it is operator dependent. Despite its high sensitivity in assessing malignancy risk, ultrasonography has limited specificity, and further evaluation using FNAC is required to confirm malignancy [1,8]. Although ultrasound is an excellent test for the diagnosis of thyroid nodules, there is a growing enthusiasm for innovative diagnostic techniques that can enhance both sensitivity and specificity. There is a high interest in a better way to detect cancer with precision while minimizing unnecessary testing, thereby refining patient care.

Performing FNAC on all nodules detected by ultrasonography is impractical, as it may increase healthcare costs due to unnecessary testing and cause patient discomfort from invasive procedures. Although FNAC is useful for distinguishing between benign and malignant thyroid nodules, performing it on all nodules is considered an unnecessary utilization of healthcare resources [9,10]. FNAC is a safe, simple, and cost-effective diagnostic method for evaluating thyroid nodules, playing a critical role in the selection of surgical, interventional or conservative management [11]. However, there has been a problem with over-diagnosis and over-treatment due to the slow growth and lower invasiveness of many thyroid cancers [12].

To enhance diagnostic accuracy and reduce unnecessary interventions, andvanced imaging methods such as elastography and AI-based diagnostic tools have been introduced [13]. Elastography is a real-time, non-invasive imaging technique that assesses tissue stiffness by measuring the degree of deformation under applied pressure. This advanced computer-aided diagnosis (CAD) technology operates on the principle that softer areas deform more easily than firmer areas when pressure is applied [14]. The ECI quantitatively assesses the stiffness contrast between the nodule and surrounding normal tissue and is a useful index for the evaluation of malignancy risk [15].

Meanwhile, S-detect is a deep learning-based computer-aided diagnosis (DL-CAD) system that analyzes grayscale 2D ultrasound images to evaluate the morphological characteristics of thyroid nodules, providing a visual guide to the likelihood of malignancy [16,17]. Both ECI and S-detect contribute to a more precise characterization of thyroid nodules and facilitate appropriate treatment planning by providing data on the elasticity and morphological characteristics of nodules, respectively. These technologies offer objective, reproducible data that may overcome the limitations of subjective visual interpretation in conventional ultrasound.

Ultrasonography of the thyroid relies on visual assessment, meaning that the accuracy of diagnosis can vary based on the experience and skill of the examiner. We hypothesize that both ECI and S-detect have the potential to serve as adjunctive or alternative diagnostic tools to FNAC in selected clinical scenarios, especially where noninvasive decision-making is prioritized. This study aims to evaluate the diagnostic performance and clinical utility of these modalities in differentiating between benign and malignant thyroid nodules. Furthermore, we seek to explore how their implementation could contribute to reducing the number of unnecessary invasive procedures and ultimately improve diagnostic efficiency and patient care.

2. Materials and Methods

2.1. Study Design and Population

This study enrolled 159 outpatients (61 male and 98 female) aged 30–83 years (56.14±11.35) who visited J Internal Medicine Clinic in Busan from January 2023 to June 2024. A cohort of 194 patients

Peer-reviewed version available at Diagnostics 2025, 15, 2191; doi:https://doi.org/10.3390/diagnostics15172191

with thyroid nodules underwent evaluations including thyroid ultrasound etc. Among them, 19 patients were excluded due to Bethesda Category 1 (Non-diagnostic) cytology resulting from insufficient specimens. Additionally, 16 patients with Bethesda Category 3 (Atypia/follicular lesion of undetermined significance) were excluded due to the inherent diagnostic uncertainty and lack of confirmatory histopathology. Ultimately, 159 patients (61 males and 98 females) were included in the final analysis. The study's flowchart is depicted in Figure 1.

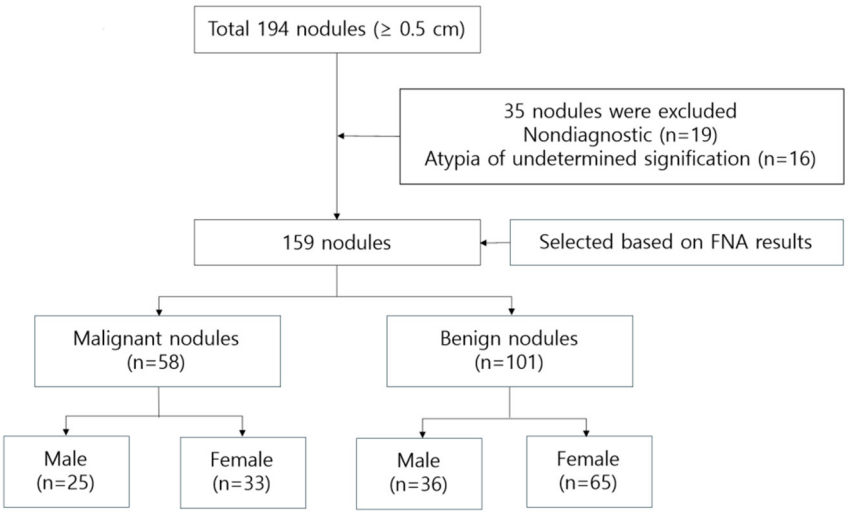

Figure 1. Flowchart of the study population.

Participants underwent FNAC after a new diagnosis of one or more thyroid nodules. Patients who had previously undergone thyroid surgery, were currently undergoing treatment for thyroid-related conditions, or had nondiagnostic or unsatisfactory FNAC results due to inadequate sampling were excluded from the study [18]. FNAC results were interpreted according to 'The Bethesda System for Reporting Thyroid Cytopathology', which classifies malignancy risk into six categories [19]. Each category has an implied cancer risk, which ranges from 1% to 3% overall for the "Benign" category to virtually 100% for the "Malignant" category [20]. Each category, based on its associated cancer risk, is linked to evidence-based clinical management guidelines, as outlined in Table 1.

Ethical approval for this study was obtained from the Institutional Bioethics Committee of University B (approval NO. CUPIRB-2024-033).

Table 1. The Bethesda system for reporting thyroid cystopathology.

Category	Meaning	Risk of malignancy(%)
I	Non-diagnostic or inadequate	1-4
II	Benign	1-3
III	Atypia/follicular lesion of undetermined significance	5-15
IV	Follicular neoplasm or suspicious for follicular neoplasm	20-30
V	Suspicious for malignancy	60-75
VI	Malignant	97-99

2.2. Ultrasound Examination

Thyroid nodule detection was performed using a high-resolution ultrasound system (RS85, Samsung Medison, Seoul, South Korea) with a 14 MHz high-frequency linear transducer (LA 2-14A, Samsung Medison). An ultrasound technologist with over 20 years of clinical experience conducted the ultrasound examinations, and a radiologist interpreted the images based on the guidelines of the Korean Thyroid Imaging Reporting and Data System (K-TIRADS). An internal medicine specialist with 20 years of experience performed the FNAC procedure according to the K-TIRADS guidelines.

Peer-reviewed version available at *Diagnostics* **2025**, *15*, 2191; doi:https://doi.org/10.3390/diagnostics15172191

Each case involved more than three punctures, and the final diagnoses were confirmed by a certified pathologist [21,22].

2.3. Elastography

For the elastography procedure, patients were positioned supine with their heads slightly turned away from the thyroid being examined and their chin extended. B-mode ultrasound images of the thyroid nodule were acquired, and static elastography was performed [23]. Images were obtained by using light pressure to ensure patient comfort, and ECI was automatically measured within the region of interest. The ECI is derived using the E-Thyroid software, which employs a steady-state quasi-static physiological excitation technique. This method leverages the carotid pulsation as a strain inducer to achieve a quantitative evaluation of tissue stiffness [24]. The relevant case is depicted in Figure 2.

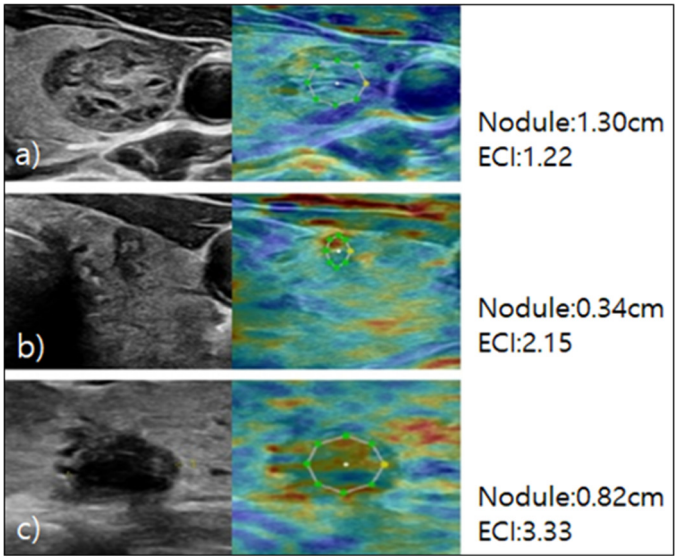

Figure 2. a) Isoechoic, well-defined margin and spongiform nodule localized in the left lobe of the thyroid gland. The axial peri-intranodular ECI was 1.22. Histology confirmed the diagnosis of benign nodular hyperplasia. b) Hypoechoic nodule with taller than wider and some internal calcifications localized in the left lobe of the thyroid gland. The axial peri-intranodular ECI was 2.15. Histology confirmed the diagnosis of papillary carcinoma. c) Hypoechoic nodule with irregular margins and some internal calcifications localized in middle portion of the thyroid gland. Peri-intranodular ECI measures 3.33. Histology confirmed the diagnosis of papillary carcinoma.

2.4. S-Detect

S-detect is an AI-based CAD software designed for ultrasound image analysis. Upon establishing the region of interest (ROI) for the targeted nodule, the software automatically delineates the boundaries and initiates the analysis [21,25]. If there errors the boundaries delineated by the software, manual delineation of the boundaries was performed. First of all, conventional ultrasound scanning was performed. After freezing of a static ultrasound image of the thyroid nodule, the ROI was manually set around the lesion, and S-detect was subsequently utilized to analyze the lesions. The nodules were then classified as “possibly benign” or “possibly malignant” based on characteristics such as internal composition, echogenicity, orientation, margin, and shape. All classifications rendered by S-detect (“possibly benign” or “possibly malignant”) were independently reviewed by an internal medicine specialist with over 20 years of experience in thyroid imaging. This procedure is depicted in Figure 3 and Figure 4.

We also noted that the S-detect software (Samsung Medison Co., Ltd.) used in this study has been validated in previous studies that demonstrated its diagnostic reliability and accuracy in

Peer-reviewed version available at Diagnostics 2025, 15, 2191; doi:https://doi.org/10.3390/diagnostics15172191

differentiating benign from malignant thyroid nodules [16,21]. These prior studies served as the basis for its clinical implementation in our study setting.

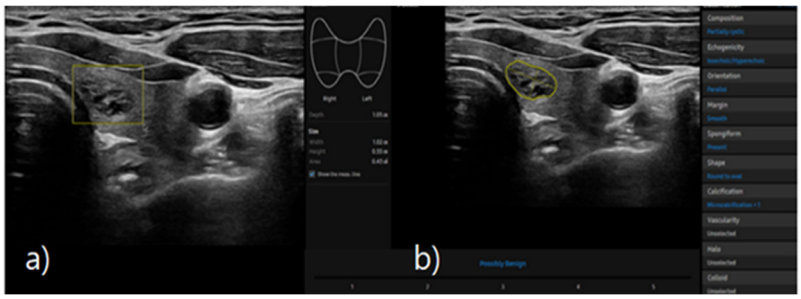

Figure 3. a) Ultrasound grayscale transverse image of the left thyroid lobe in a 57-year-old woman. b) Thyroid nodule automatically classified as "possibly benign" using S-detect according to characteristics such as internal composition, echogenicity, orientation, margin, and shape.

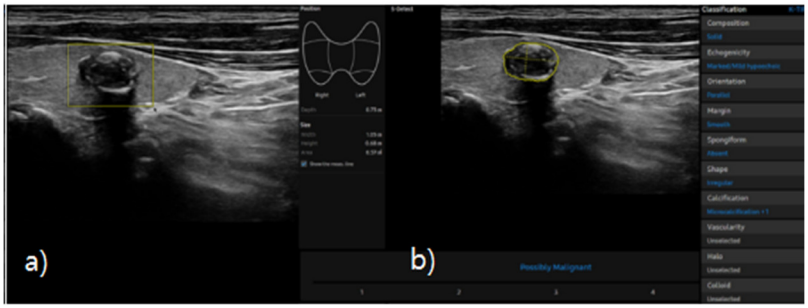

Figure 4. a) Ultrasound grayscale longitudinal image of the left thyroid lobe in a 69-year-old man. b) Thyroid nodules automatically classified as "possible malignant" using S-detect according to characteristics such as internal composition, echogenicity, orientation, margin, and shape.

2.5. Statistical Analysis

The general characteristics of the study population are presented as mean and standard deviation (SD) or number of persons (n) and percentage (%). The necessity of the ROC curve lies in finding a classification model that achieves a suitable balance while minimizing false positives (predicting a negative as positive) and false negatives (predicting a positive as negative). To assess the diagnostic utility of elastography, receiver operating characteristic (ROC) curve analysis was conducted, and the area under the curve (AUC), positive predictive value (PPV), negative predictive value (NPV), sensitivity, and specificity were calculated. For reliability assessment, diagnostic agreement with FNAC results was evaluated using Cohen's Kappa analysis. Statistical significance was set at $p<0.05$, and all analyses were performed using SPSS Version 29.0 (IBM Corp., Armonk, NY, USA).

3. Results

3.1. General Characteristics of Patients

Based on FNAC results, 101 patients (63.5%) had benign nodules, and 58 patients (36.5%) had malignant nodules. The cohort included 61 (38.4%) males and 98 (61.6%) females, with no significant difference in sex distribution between the benign and malignant groups ($p=0.352$). The mean age of the study population was 56.14±11.35 years. The nodules' average size was confirmed to be 1.07±0.85 cm, with a statistically significant difference observed between benign (1.23±0.94 cm) and malignant (0.79±0.58 cm) nodules ($p=0.002$). In terms of nodule composition, 146 (91.8%) were solid, 11 (6.9%) were predominantly solid, and 2 (1.3%) were predominantly cystic, with no significant difference between the benign and malignant groups ($p=0.077$). Regarding echogenicity, 119 nodules (74.8%)

Peer-reviewed version available at *Diagnostics* **2025**, *15*, 2191; doi:https://doi.org/10.3390/diagnostics15172191

were hypoechoic, and 40 (25.2%) were isoechoic; no hyperechoic nodules were identified (p<0.001). Regarding nodule orientation, 105 (66.0%) were parallel, and 54 (34.0%) were nonparallel, with nonparallel orientation being more frequently observed in malignant cases (p<0.001). In terms of nodule margins, 75 nodules (47.2%) were circumscribed, and 84 (52.8%) were not circumscribed, with circumscribed margins being more common in benign nodules and not circumscribed margins in malignant ones (p<0.001). Regarding shape, 67 nodules (42.1%) were oval, 34 (21.4%) were round, and 58 (36.5%) were irregular, with irregular shapes being more frequently associated with malignancy (p<0.001). Calcification was present in 111 nosules (69.8%) and absent in 48 (30.2%), showing a significant difference between the two groups (p<0.001). Posterior shadowing was observed in 131 nodules (82.4%), while 28 (17.6%) showed no shadowing (p=0.021). The results are detailed in Table 2.

Table 2. Comparison of characteristics between benign and malignant nodules (n=159).

Variable		n(%)	Benign	Malignant	χ^2/t	*p* value
Sex	Male	61(38.4)	36(22.7)	25(15.7)	0.87	0.352
	Female	98(61.0)	65(40.5)	33(20.5)		
Age(year)		56.14±11.35	56.53±10.29	55.45±13.06	0.54	0.021
Size(cm)		1.07±0.85	1.23±0.94	0.79±0.58	3.58	0.002
Composition	Solid	146(91.8)	89(56.0)	57(35.8)	5.12	0.077
	Predominantly solid	11(6.9)	10(6.3)	1(0.6)		
	Predominantly cystic	2(1.3)	2(1.3)	0(0.0)		
Echogenicity	Hypoechogenicity	119(74.8)	62(39.0)	57(35.8)	26.63	<0.001
	Isoechogenicity	40(25.2)	39(24.6)	1(0.6)		
Orientation	Parallel	105(66.0)	82(51.5)	23(14.5)	28.34	<0.001
	Nonparallel	54(34.0)	19(12.0)	35(22.0)		
Margin	Circumscribed	75(47.2)	64(40.3)	11(6.9)	29.99	<0.001
	Not circumscribed	84(52.8)	37(23.3)	47(29.5)		
Shape	Oval	67(42.1)	60(37.7)	7(4.4)	36.84	<0.001
	Round	34(21.4)	19(12.0)	15(9.4)		
	Irregular	58(36.5)	22(13.8)	36(22.7)		
Calcification	Presence	111(69.8)	82(51.6)	29(18.2)	17.00	<0.001
	Absence	48(30.2)	19(12.0)	29(18.2)		
Posterior shadow	Presence	131(82.4)	89(56.0)	42(26.4)	6.26	0.012
	Absence	28(17.6)	12(7.5)	16(10.1)		
Total		159(100)	101(63.5)	58(36.5)		

Unit: Person (%), Mean ± SD.

3.2. Performance of Diagnostic Models

In the ROC curve analysis, S-detect had an AUC of 0.78 (95% CI 0.72–0.84, p<0.001), sensitivity of 87.93%, specificity of 68.32%, PPV of 61.4%, and NPV of 90.8%. For ECI, the optimal cutoff value was 2.41 and had an AUC of 0.85 (95% CI 0.79–0.90, p<0.001), sensitivity of 87.93%, specificity of 81.19%, PPV of 72.9%, and NPV of 92.1%. Radiologist evaluation had an AUC of 0.89 (95% CI 0.84–0.93, p<0.001), sensitivity of 98.28%, specificity of 79.21%, PPV of 73.1%, and NPV of 98.8%. The results are presented in Table 3 and Figure 5.

Table 3. Evaluation of the diagnostics performed by S-detect, ECI, and a radiologist.

Variable	AUC (95% CI)	Sensitivity	Specificity	Youden index	PPV	NPV	*p* value
S-detect	0.78	87.93	68.32	0.562	61.4	90.8	<0.001

Peer-reviewed version available at Diagnostics 2025, 15, 2191; doi:https://doi.org/10.3390/diagnostics15172191

	(0.72–0.84)						
ECI	0.85 (0.79–0.90)	87.93	81.19	0.773	72.9	92.1	<0.001
Radiologist	0.89 (0.84–0.93)	98.28	79.21	0.775	73.1	98.8	<0.001

ECI, elasticity contrast index; AUC, area under curve; CI, confidence interval; PPV, positive predictive value; NPV, negative predictive value.

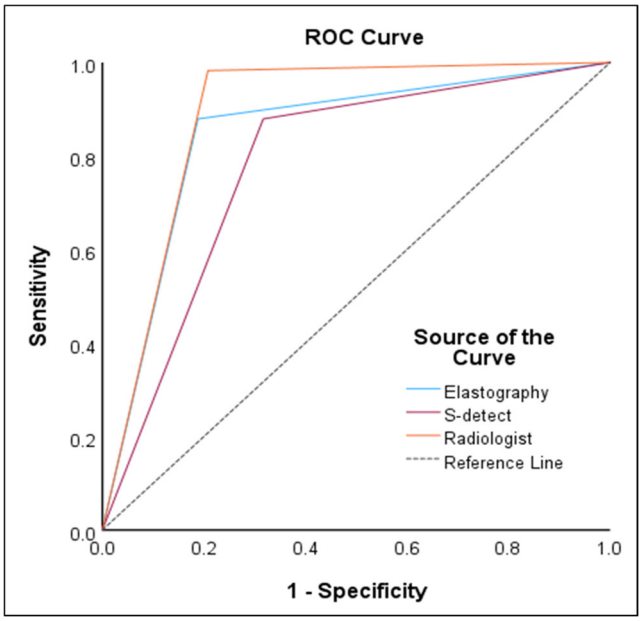

Figure 5. Receiver operating characteristic curve analysis comparing the diagnostic performance of the radiologist, S-detect, and elastography based on fine needle aspiration cytology results.

3.3. Agreement of Diagnostic Models

To evaluate the diagnostic agreement of each modality with the reference standard (FNAC), Cohen's Kappa coefficients were calculated. Based on the widely accepted classification by Landis and Koch, Kappa values were interpreted as follows: values of 0.41-0.60 indicate moderate agreement, and 0.61-0.80 indicate substantial agreement. According to this scale, S-detect exhibited moderate agreement (Kappa value of 0.52, 95% CI 0.38–0.64, p<0.001), while ECI showed substantial agreement (Kappa value of 0.66, 95% CI 0.54–0.78, p<0.001). K-TIRADS evaluation by an internist also demonstrated substantial agreement (Kappa value of 0.72, 95% CI 0.62–0.83, p<0.001) [26]. These finding suggest that both ECI and K-TIRADS achieved higher diagnostic consistency with FNAC compared to S-detect. All agreements were statistically significant, underscoring the clinical reliability of these modalities. The detailed results are summarized in Table 4.

Table 4. Diagnostic agreement of S-detect, ECI, and radiologist based on FNAC (n=159).

Variable	Kappa	SE	95% CI	p value
S-detect	0.52	0.06	0.38~0.64	<0.001
ECI	0.66	0.06	0.54~0.78	<0.001
Radiologist	0.72	0.05	0.62~0.83	<0.001

SE, standard error; CI, confidence interval; ECI, elasticity contrast index.

4. Discussion

Thyroid nodules are generally slow-growing and often do not require surgical intervention. According to the National Cancer Registry Statistics in South Korea, the 5-year relative survival rate

Peer-reviewed version available at Diagnostics 2025, 15, 2191; doi:https://doi.org/10.3390/diagnostics15172191

(2016–2020) for thyroid cancer is 100% [27]. With early detection and appropriate treatment, malignant thyroid nodules have a favorable prognosis compared to other cancers [28]. Additionally, avoiding unnecessary tests and surgeries for benign nodules helps reduce healthcare costs and improves patients' quality of life [29,30]. Therefore, distinguishing between benign and malignant nodules at an early stage is crucial.

There has been ongoing research to incorporate AI-based computer-aided diagnostic systems into ultrasound examinations to minimize diagnostic variability among clinicians caused by differences in proficiency and provide consistent treatment recommendations [31,32]. In this study, we compared the diagnostic performance of radiologist evaluation (K-TIRADS) with AI-based S-detect and ECI (elastography) to examine their potential as adjunctive diagnostic tools.

In this study, the diagnostic accuracy was the highest for K-TIRADS based radiologist evaluation, with an accuracy of 89%, sensitivity of 98.28%, specificity of 79.21%, PPV of 73.1%, and NPV of 98.8%. Next, the accuracy of ECI was relatively high at 85%, with a sensitivity of 87.93%, specificity of 81.19%, PPV of 72.9%, and NPV of 92.1%, indicating that ECI can be helpful in differentiating thyroid nodules. The accuracy of S-detect was the lowest among the diagnostic models, at 78%, with a sensitivity of 87.93%, specificity of 68.32%, PPV of 61.4%, and NPV of 90.8%. According to Cho et al. [33], the diagnostic accuracy of combined grayscale ultrasound and ECI was 78.6% when using an ECI cutoff value of 3.5, which was higher than that of grayscale ultrasound (76.9%) and ECI alone (67.1%). Sheng et al. [34] reported that ECI significantly increases in patients with Hashimoto's thyroiditis and can be used to assess the degree of immune dysfunction. Di et al. [35] found that the optimal ECI cutoff value was 2.16, lower than the 2.41 found in this study, with a sensitivity of 90.3%, specificity of 82.9%, PPV of 83.7%, and NPV of 91.2%. The said study suggested that these variations could be attributed to differences in study populations or diagnostic criteria, confirming that ECI can be a useful tool for assessing the malignant potential of thyroid nodules in specific contexts. In addition, the authors of the said study suggest that elastography, which measures tissue stiffness upon external pressure in real-time through noninvasive methods, is a useful tool for differentiating thyroid nodules [35,36].

S-detect showed lower diagnostic accuracy compared to ECI and radiologist interpretation. This may be due to its exclusive dependence on grayscale ultrasound images, potentially limiting its ability to account for tissue stiffness or vascularity. Additionally, variations in image acquisition or nodule characteristics may affect performance. These findings are in line with previous research suggesting that AI-based tools show improved diagnostic value when used in conjunction with other imaging modalities or expert review [37,38].

A limitation of this study is the lack of an objective criterion for accurately measuring the degree of fine pressure applied during elastography, which might have led to variability in the elasticity grades assigned by each examiner [39]. In addition, the sample size was limited to 159 subjects, and the study was conducted in a single geographic area, which may limit the generalizability of the results. To address these limitations, larger-scale studies involving diverse population groups are necessary. Moreover, educational programs to enhance examiner proficiency, research aimed at improving diagnostic accuracy through the development of objective measurement criteria for elastography, and advancements in artificial intelligence-based diagnostic tools should continue. Despite these limitations, elastography has proven to be a valuable noninvasive diagnostic tool for thyroid nodules. The Kappa coefficient of 0.66 observed in this study indicates substantial agreement with FNAC results, suggesting that elastography could play an important role in the development and refinement of diagnostic techniques for thyroid nodules [40,41]. The results of this study show that ECI, as calculated through elastography, demonstrated relatively high sensitivity and specificity. Although S-detect's accuracy was lower compared to the other two methods, it still shows promise as an artificial intelligence-based diagnostic tool for thyroid nodule evaluation.

Elastography and S-detect demonstrated superior diagnostic performance over conventional B-mode ultrasonography by enhancing tissue stiffness quantification and providing algorithm-based interpretation, respectively. These modalities may contribute to improved diagnostic accuracy and

Peer-reviewed version available at Diagnostics 2025, 15, 2191; doi:https://doi.org/10.3390/diagnostics15172191

reproducinility in the evaluation of thyroid nodules, particularly those with indeterminate sonographic features.

5. Conclusions

This study evaluated the diagnostic performance of elastography and AI-based S-detect as adjunctive tools for thyroid nodule assessment. These technologies enable rapid, objective analysis of ultrasound images, thereby enhancing diagnostic efficiency and supporting clinicians in making more accurate and consistent decisions.

Although elastography and S-detect cannot fully replace FNAC, their combined use significantly improves the accuracy and reliability of thyroid nodule diagnosis. This may contribute to reducing unnecessary FNAC and biopsy procedures, particularly in low-risk cases, ultimately improving patient comfort and resource utilization.

However, before these tools can be widely adopted in routine clinical practice, several limitations must be addressed. These include the retrospective, single-center design of the study, operator dependency in elastography, and the limited interpretation of AI algorithms. Furthermore, the diagnostic performance in indeterminate nodules and long-term clinical outcomes were not evaluated.

To establish broader applicability, future research should include large-scale, multi-center prospective studies across diverse populations and nodule types. Technological refinements such as improved deep learning algorithms, multi-modal integration, and real-time feedback may further enhance diagnostic precision. Additionally, structured education and training programs are essential to ensure consistent and effective clinical implementation.

In conclusion, the integration of elastography and S-detect into ultrasound workflows holds promise for improving diagnostic accuracy, reducing unnecessary invasive procedures, and optimizing thyroid cancer management.

Author Contributions: Conceptualization, J.Y.P. and S.H.Y.; methodology, S.H.Y.; formal analysis, S.H.Y.; investigation, J.Y.P.; data curation, J.Y.P.; writing—original draft preparation, J.Y.P. and S.H.Y.; writing—review and editing, J.Y.P. and S.H.Y.; visulalization, J.Y.P; funding acquisition, S.H.Y. All authors have read and agreed to the published version of the manuscript.

Funding: This research received no external funding.

Institutional Review Board Statement: Ethical approval for this study was obtained from the Institutional Bioethics Committee of University B (approval NO. CUPIRB-2024-033).

Informed Consent Statement: The requirement for patient consent was waived due to the study's retrospective nature.

Data Availability Statement: The data supporting the findings of this study are available on request from the corresponding author (S.H.Y.).

Conflicts of Interest: The authors declare no conflicts of interest.

Abbreviations

FNAC	fine niddle aspiration cytology
PPV	positive predictive value
NPV	negative predictive value
CAD	computer-aided diagnosis
ECI	elasticity contrast index
DL-CAD	deep learning-based computer-aided diagnosis
K-TIRADS	Korean Thyroid Imaging Reporting and Data System
SD	standard deviation
ROC	receiver operating characteristic

Peer-reviewed version available at Diagnostics 2025, 15, 2191; doi:https://doi.org/10.3390/diagnostics15172191

AUC	area under the curve
CI	confidence interval
SE	standard error

References

1. Park, Y.J.; Lee, E.K.; Song, Y.S.; Koo, B.S.; Kwon, H.; Kim, K.; Kim, M.; Kim, B.H.; Kim, W.G.; Kim, W.B.; et al. Korean Thyroid Association Guidelines on the Management of Differentiated Thyroid Cancer; Overview and Summary 2024. *Int J Thyroidol* **2024**, *17*, 1–20. DOI:10.11106/ijt.2024.17.1.1.
2. Hegedüs, L. Clinical practice: The thyroid nodule. *N Engl J Med* **2004**, *351*, 1764–1771. DOI:10.1056/NEJMcp031436.
3. Kim, K.H.; Kim, E.K.; Kwak, J.Y.; Kim, M.J. *Detection and Management of Thyroid Incidentaloma*; Vol. 27; Korean Society of Ultrasound in Medicine, 2008; pp. 111–117.
4. Shaheen, R.; Levine, D. *Diagnostic Ultrasound* ed. 5; Elsevier: Philadelphia, 2018; pp. 725–765.
5. AlSaedi, A.H.; Almalki, D.S.; ElKady, R.M. Approach to thyroid nodules: diagnosis and treatment. *Cureus* **2024**, 16, e52232. DOI: 10.7759/cureus.52232.
6. Dighe, M.; Barr, R.; Bojunga, J.; Cantisani, V.; Chammas, M.C.; Cosgrove, D.; Cui, X.W.; Dong, Y.; Fenner, F.; Radzina, M.; et al. Thyroid ultrasound: State of the art Part 2. *Med Ultrason* **2017**, *19*, 195–210. DOI:10.11152/mu-999.
7. Hahn, S.Y.; Shin, J.H.; Oh, Y.L.; Son, Y.I. Discrepancies between the ultrasonographic and gross pathological size of papillary thyroid carcinomas. *Ultrasonography* **2016**, *35*, 220–225. DOI:10.14366/usg.15077.
8. Tian, W.; Hao, S.; Gao, B.; Jiang, Y.; Zhang, S.; Guo, L.; Luo, D. Comparison of diagnostic accuracy of real-time elastography and shear wave elastography in differentiation malignant from benign thyroid nodules. *Med (Baltim)* **2015**, *94*, e2312. DOI:10.1097/MD.0000000000002312.
9. Lee, Y.J.; Kim, D.W.; Park, Y.M.; Park, H.K.; Jung, S.J.; Kim, D.H.; Lee, S.M.; Oh, M. Comparison of sonographic and cytological diagnoses of solid thyroid nodules:Empahsis on the discordant cases. *Diagn Cytopathol* **2015**, 43, 953–959. DOI:10.1002/dc.23363.
10. Dondi, F.; Gatta, R.; Treglia, G.; Piccardo, A.; Albano, D.; Camoni, L.; Gatta, E.; Cavadini, M.; Cappelli, C.; Bertagna, F. Application of radiomics and machine learning to thyroid diseases in nuclear medicine: a systematic review. *Rev Endocr Metab Disord* **2024**, 25, 175–186. DOI:10.1007/s11154-023-09822-4.
11. Dietrich, C.F.; Muller, T.; Bojunga, J.; Dong, Y.; Mauri, G.; Radzina, M.; Dighe, M.; Cui, X.W.; Grunwald, F.; Schuler, A.; Ignee, A.; Korkusuz, H. Statement and Recommendations on Inerventional Ultrasound as a Thyroid Diagnostic and Treatment Procedure. *Ultrasound Med Biol* **2018**, 44, 14-36.
12. Ahn, H.S.; Kim, H.J.; Welch, H.G. Korea's thyroid-cancer "epidemic"--screenign and overdiagnosis. *N Engl J Med* **2014**, 371, 1765-1767. DOI:10.1056/NEJMp1409841.
13. Ha, E.J.; Baek, J.H. Applications of machine learning and deep learning to thyroid imaging: Where do we stand? *Ultrasonography* **2021**, *40*, 23–29. DOI:10.14366/usg.20068.
14. Zhao, C.K.; Xu, H.X. Ultrasound elastography of the thyroid: Principles and current status. *Ultrasonography* **2019**, *38*, 106–124. DOI:10.14366/usg.18037.
15. Cong, P.; Wang, X.M.; Zhang, Y.F. Comparison of artificial intelligence, elastic imaging, and the thyroid imaging reporting and data system in the differential diagnosis of suspicious nodules. *Quant Imaging Med Surg* **2024**, *14*, 711–721. DOI:10.21037/qims-23-788.
16. Ko, E.Y. S-detect in breast ultrasound: Initial experience. *Samsung Medical Center, Medison, (Seoul, Korea)*. Available online: http://www.samsung.com/global/business.
17. Sorrenti, S.; Dolcetti, V.; Radzina, M.; Bellini, M.I.; Frezza, F.; Munir, K.; Grani, G.; Durante, C.; D'Andrea, V.; David, E.; et al. Artificial intelligence for thyroid nodule characterization: Where are we standing? *Cancers (Basel)* **2022**, *14*, 3357. DOI:10.3390/cancers14143357.
18. Colakoglu, B.; Yildirim, D.; Alis, D.; Ucar, G.; Samanci, C.; Ustabasioglu, F.E.; Bakir, A.; Ulusoy, O.L. Elastography in distinguishing benign from malignant thyroid nodules. *J. Clin. Imaging Sci.* **2016**, 6, 51. DOI:10.4103/2156-7514.197074.

Peer-reviewed version available at *Diagnostics* **2025**, *15*, 2191; doi:https://doi.org/10.3390/diagnostics15172191

19. Ali, S.Z.; Valoch, Z.W.; Cochand-Priollet, B.; Schmitt, F.C.; Vielh, P.; VanderLaan, P.A. The 2023 Bethesda System for Reporting Thyroid Cytopathology. *Thyroid* **2023**, 33, 1039-1044. DOI:10.1089/thy.2023.0141.
20. Cibas, E.S.; Ali, S.Z. The Bethesda System for Reporting Thyroid Cytopathology. *American Journal of Clinical Pathology* **2009**, 132, 658-665. DOI:10.1309/AJCPPHLWMI3JV4LA.
21. Park, J.Y.; Cho, Y.I.; Yang, S.H. Diagnostic usefulness of deep learning based S-detect using thyroid ultrasonography. *Next-Gener Converg Technol Assoc* **2024**, *8*, 343–350. DOI:10.33097/JNCTA.2024.08.2.343.
22. Ha, E.J.; Chung, S.R.; Na, D.G.; Ahn, H.S.; Chung, J.; Lee, J.Y.; Park, J.S.; Yoo, R.E.; Baek, J.H.; Baek, S.M.; et al. 2021 Korean thyroid imaging reporting and data system and imaging-based management of thyroid nodules: Korean society of thyroid radiology consensus statement and recommendations. *Korean J Radiol* **2021**, *22*, 2094–2123. DOI:10.3348/kjr.2021.0713.
23. Ophir, J.; Garra, B.; Kallel, F.; Konofagou, E.; Krouskop, T.; Righetti, R.; Varghese, T. Elastographic imaging. *Ultrasound Med Biol* **2000**, *26*(1) Supplement 1, S23–S29. DOI:10.1016/S0301-5629(00)00156-3.
24. Cho, Y.J.; Ha, E.J.; Han, M.R.; Choi, J.W. US elastography using carotid artery pulsation may increase the diagnostic accuracy for thyroid nodules with US-pathology discordance. *Ultrasound Med Biol* **2017**, 43, 1587-1595. DOI:10.1015/j.ultrasmedbio.2017.04.007.
25. Russ, G.; Bonnema, S.J.; Erdogan, M.F.; Durante, C.; Ngu, R.; Leenhardt, L. European Thyroid association guidelines for ultrasound malignancy risk stratification of thyroid nodules in adults: The EU-TIRADS. *Eur Thyroid J* **2017**, *6*, 225–237. DOI:10.1159/000478927.
26. Landis, J.R.; Koch, G.G. The measurement of observer agreement for categorical data. *Biometrics* **1977**, *33*, 159–174. DOI:10.2307/2529310.
27. Korea Central Cancer Registry, National Cancer Center. Annual Report of Cancer Statistics in Korea in 2020; Ministry of Health and Welfare. Available online: https://www.ncc.re.kr/cancerStatsList.ncc.
28. Hong, Y.; Liu, X.; Li, Z.; Zhang, X.; Chen, M.; Luo, Z. Real-time ultrasound elastography in the differential diagnosis of benign and malignant thyroid nodules. *J Ultrasound Med* **2009**, *28*, 861–867. DOI:10.7863/jum.2009.28.7.861.
29. Yang, S.H.; Lee, J.S. Evaluation of breast ultrasound lesion recognition rate using machine learning application. *Next-Gener Converg Technol Assoc* **2023**, *7*, 1261–1267.
30. Genere, N.; Hurtado, M.D.; Cortes, T.; Athimulam, S.; Al Ward, R.; Callstrom, M.R.; Stan, M.n.; Morris, J.C.; Brito, J.p. Drivers of the decision to biopsy and follow-up of small suspicious thyroid nodules. *Endocr. Pract.* **2020**, 26, 857-868. DOI:10.4158/EP-2019-0590.
31. Park, S.H.; Kim, S.J.; Kim, E.K.; Kim, M.J.; Son, E.J.; Kwak, J.Y. Interobserver agreement in assessing the sonographic and elastographic features of malignant thyroid nodules. *AJR Am J Roentgenol* **2009**, *193*, 416–423.
32. Kim, H.L.; Ha, E.J.; Han, M. Real-World Performance of Computer-Aided Diagnosis System for Thyroid Nodules Using Ultraosonography. *Ultrasound Med Biol* **2019**, 45, 2672-2678.
33. Cho, Y.J.; Ha, E.J.; Han, M.R.; Choi, J.W. US elastography using carotid artery pulsation may increase the diagnostic accuracy for thyroid nodules with US-pathology discordance. *Ultrasound Med Biol* **2017**, *43*, 1587–1595. DOI:10.1016/j.ultrasmedbio.2017.04.007.
34. Sheng, J.G.; Wang, B.; Cao, K.K.; Zhang, S. Relationship of thyroid ultrasound elasticity contrast index with serum autoantibody and Th1/Th2 cytokine levels in patients with Hashimoto's thyroiditis. *J Hainan Med Univ* **2016**, *22*, 147–150.
35. Di, Z.; Li, Z.; Tian, J.; Wang, D.; Liu, L.; Liu, C. The value of elasticity contrast index in the differential diagnosis of thyroid solid nodules. *Ultrasound Q* **2019**, *35*, 259–263. DOI:10.1097/RUQ.0000000000000457.
36. Aghaghazvini, L.; Maheronnaghsh, R.; Soltani, A.; Rouzrokh, P.; Chavoshi, M. Diagnostic value of shear wave sonoelastography in differentiation of benign from malignant thyroid nodules. *Eur J Radiol* **2020**, 126, 108926.
37. Du, Y.R.; Ji, C.L.; Wu, Y.; Gu, X.G. Combination of ultrasound elastography with TI-RADS in the diagnosis of small thyroid nodules (≤10 mm): A new method to increase the diagnostic performance. *Eur J Radiol* **2018**, 109, 33-40. DOI:10.1016/j.ejrad.2018.10.024.

Peer-reviewed version available at *Diagnostics* **2025**, *15*, 2191; doi:https://doi.org/10.3390/diagnostics15172191

38. Wang, F; Chang, C.; Chen, M.; Cao, Y.; Chen, Y.L.; Zhou, S.C.; Li, J.W.; Zhi, W.X. Does lesion size affect the value of shear wave elastography for differentiating between benign and malignant thyroid nodules? *J Ultrasound Med* **2018**, 37, 601-609. DOI:10.1002/jum.14367.
39. Han, R.J.; Du, J.; Li, F.H.; Zong, H.R.; Wang, J.D.; Shen, Y.L.; Zhou, Q.Y. Comparisons and combined application of two-dimensional and three-dimensional real-time shear wave elastography in diagnosis of thyroid nodules. *J Cancer* **2019**, *10*, 1975–1984. DOI:10.7150/jca.30135.
40. Reverter, J.L.; Vázquez, F.; Puig-Domingo, M. Diagnostic performance evaluation of computer-assisted imaging analysis system for ultrasound risk stratification of thyroid nodules. *AJR Am J Roentgenol* **2019**, *213*, 169–174. DOI:10.2214/AJR.18.20740.
41. Gao, L.; Liu, R.; Jiang, Y.; Song, W.; Wang, Y.; Liu, J.; Wang, J.; Wu, D.; Li, S.; Hao, A.; Zhang, B. Computer-aided system for diagnosing thyroid nodules on ultrasound: A comparison with radiologist-based clinical assessments. Head Neck 2018, 40, 778-783. DOI:10.1002/hed.25049.